JOURNAL OF AIRCRAFT
Vol. 40, No. 1, January–February 2003

Optimization of an Aircraft Power Distribution Subsystem

S. Chandrasekaran*
Rockwell Science Center, Thousand Oaks, California 91358-4017
and
S. A. Ragon,† D. K. Lindner,‡ Z. Gürdal,§ and D. Boroyevich¶
Virginia Polytechnic Institute and State University, Blacksburg, Virginia 24061

A mathematical optimization problem is formulated to design several components of an electrical power distribution system for next-generation aircraft. A simple interconnected system consisting of an input filter and a dc–dc buck converter is used as the prototype for the optimization demonstration. The components are designed for minimum weight, subject to performance, stability, and peak voltage constraints. Optimized designs for each of the individual subsystems and for the integrated system are presented. It is shown that there is an interaction between the filter design problem and the converter design problem and that weight improvements can be obtained by considering these interactions. The optimization methodology described enables designers to obtain optimized electric power subsystem designs in a time-efficient manner.

Nomenclature

A_{cp1}, A_{cp2}, A_{cpd}	=	cross-sectional area of inductor winding
$A_v(j\omega)$	=	audiosusceptibility transfer function
B_{sp}	=	saturation flux density of ferrite core material
C,C_1, C_2	=	capacitances
C_w, C_{w1}, C_{w2}, C_{wd}	=	center leg width of inductor core
D	=	converter duty cycle
F_c	=	winding pitch factor of EE core
F_w	=	window fill factor of EE core
f_s	=	switching frequency of converter
g_m	=	gain margin of converter closed loop
h_o, w_z, w_p, h_{ii}, h_{ip}	=	controller parameters of converter
I_B	=	converter average input current
$I_{L(pk)}$	=	peak inductor current
I_o	=	converter average load current
I_p	=	peak value of pulse disturbance
J	=	objective function
K_1	=	aspect ratio of center leg of EE core
K_2	=	aspect ratio of window of EE core
L, L_1, L_2, L_d	=	inductance
l_g, l_{g1}, l_{g2}, l_{gd}	=	air gap length of inductor core
n, n_1, n_2, n_d	=	number of inductor turns
R_C	=	equivalent series resistance for converter output capacitance
T_p	=	duration of pulse disturbance
V_B	=	filter output voltage
V_g	=	filter input voltage
V_o	=	converter output voltage
V_{ref}	=	reference output voltage for converter
W_a	=	window area occupied by winding
W_b	=	window area occupied by bobbin
W_{bob}	=	width of bobbin of EE core
W_C	=	capacitor weight
W_{Cu}	=	weight of copper in inductor
W_{Fe}	=	weight of iron in inductor core
W_L	=	inductor weight
W_R	=	resistor weight
W_w, W_{w1}, W_{w2}, W_{wd}	=	window width of inductor core
Z_{iB}	=	closed-loop input impedance of converter
Z_{iF}	=	input impedance of input filter
Z_{iL}	=	impedance looking out of output terminals of input filter
Z_{oB}	=	closed-loop output impedance of input filter
Z_{oC}	=	impedance looking out of input terminals of input filter
Z_{oF}	=	output impedance of input filter
α_C	=	proportionality constant for capacitor weight
ΔI_L	=	switching ripple of converter inductor current
ΔV_o	=	switching ripple of converter output voltage
Δv_B	=	transient voltage excursion at converter input
Δv_o	=	transient voltage excursion at converter output
μ_o	=	permeability of free space
ρ_{Cu}	=	density of copper
ρ_{Fe}	=	density of iron
Φ_{pk}	=	peak flux in inductor core
ϕ_m	=	phase margin of converter closed loop
ψ_{pk}	=	peak flux linkage in inductor core
ω_{cg}	=	loop gain crossover frequency of converter voltage loop
ω_p	=	passband edge frequency for input filter
ω_{s1}	=	stopband edge frequency for input filter

Received 23 January 2001; revision received 8 July 2002; accepted for publication 20 August 2002.

*Technical Staff, 1049 Camino Dois Rios.
†Research Associate, Department of Engineering Science and Mechanics. Member AIAA.
‡Associate Professor, Bradley Department of Electrical and Computer Engineering. Member AIAA.
§Professor, Departments of Aerospace and Ocean Engineering and Engineering Science and Mechanics. Associate Fellow AIAA.
¶Professor, Center for Power Electronic Systems, Bradley Department of Electrical and Computer Engineering.

I. Introduction

THE principal objective of this research effort is to develop and demonstrate optimization methods that facilitate the design of aircraft power distribution systems.[1] This approach is a departure from past design methodologies that are primarily ad hoc. The ad hoc approach to power system design is time intensive and yields components that are overdesigned to ensure global stability of the power system. The optimization methodology proposed here accounts for component interactions in the system to yield smaller, lighter weight components while maintaining performance requirements. Weight

reduction in power distribution systems may be critical for the performance of air vehicles, especially for smaller vehicles such as uninhabited surveillance and combat aircraft for which electronics systems make up a large percentage of the aircraft weight.

This optimization design methodology is proposed in anticipation of the next-generation aircraft, where it is projected that all power, with the exception of propulsion, will be distributed and processed electrically. Electrical power will be utilized for driving a diverse array of aircraft subsystems that are currently powered by hydraulic, pneumatic, or mechanical means. These subsystems include flight control actuation systems, environmental control systems, and several other utility subsystems. As the aircraft become more integrated, the coordinated, optimized design of the various subsystems will become more important. The optimization methodology introduce here is formulated in such a way as to fit into a multidisciplinary design environment.

Our primary interest is next-generation power distribution systems built around a 270-V dc distribution bus. This bus is regulated by switching power converters. Most of the loads, including the actuators, are also regulated using switching power converters. Other devices in the power system are filters and relays that serve to control the interaction of the various components of the power system. The design of the components themselves is quite complex, particularly the switching power converters. Because of their interaction with other subsystem components in the power distribution system, switching power converters can cause unstable operation of the integrated system. Hence, the global stability of the power distribution system must be accounted for in the local component design.

Similarly, the performance of the overall power distribution systems depends heavily on the interaction between the subsystems. One of the distinguishing features of these modern power distribution systems is that they allow for power flow in both the forward direction from the generator to the loads and in the reverse direction from the loads to other loads and the generator. In other words, some actuation loads in the power system are capable of regenerating power back to the source under certain operating conditions. A prime example of such a component is the actuator that drives the control surface of an aircraft. When the control surfaces reverse under air loads, the actuators can generate electric power that is fed back to the system. The process of power regeneration manifests itself as a transient disturbance on the regulated dc bus. The regenerative power causes transient voltage spikes on the dc bus. Hence, the individual component design must take into account the system level transient phenomena that occur due to the process of the regeneration of power.

Mathematical optimization techniques have found application for the design of high-performance converter and drive systems.[1–3] However, optimization methods for the design of aircraft or shipboard power distribution systems, where efficiency, size, and weight are of paramount importance, have received very little attention in the past.[4] The development of an optimization methodology for these power distribution systems is involved due to the complexity of the components and their strong interaction. Our approach to the development of a global optimization methodology is to begin with the development of an optimization methodology for the individual components of the power distribution system. The models of the individual components account for the interactions with the other components in the global system in a simplified manner. Therefore, the methodology optimizes the performance of the local component while accounting for global interactions. When the subsystems are considered jointly, the optimization formulation for each subsystem is such that they can be combined in a straightforward way to obtain an optimization methodology for the entire system.

The proposed optimization procedure is demonstrated on a simple interconnected system (henceforth referred to as the sample system) consisting of a regulated dc–dc buck converter preceded by an input filter. The sample system captures the essential features of the optimization problem formulation, which is solved using a commercially available optimization code. An optimization methodology is formulated for the filter component first. This optimization methodology is then extended to a regulated dc–dc buck converter, taking into account the increase in complexity of the converter. These two optimization problems are then combined to yield a single optimization problem for the combined system. Stability of the global system is insured, and the effects of regenerative power flow are accounted for through proper choice of constraints. To assess the validity of the results obtained from the optimizer, the optimal designs are compared to a filter built for a three-phase buck converter for a telecommunications application.[5]

The sample system is introduced in Sec. II. The optimized design of the input filter as an independent subsystem is presented in Sec. III. The optimized design of the converter as an independent subsystem is then presented in Sec. IV. The filter and converter are combined to form an interconnected system and optimized simultaneously in Sec. V. The conclusions are provided in Sec. VI.

II. Sample System

In this paper, we will demonstrate the optimization procedure on a sample system extracted from the components of a typical aircraft power distribution system. The sample system captures the salient features of the optimization problem formulation. The sample system consists of an input filter, followed by a regulated dc–dc buck converter as shown in Fig. 1.

The power is supplied by the aircraft power bus, which is assumed to be a stiff dc source of $V_g = 270$ V. The buck converter is representative of most power converters commonly found in aircraft power systems. The converter is loaded by a fixed dc current source I_o (to represent the average power drawn).

Switching converters inject an appreciable amount of high-frequency noise into the system. This high-frequency noise results in what is known as electromagnetic interference (EMI) between the converter and other interconnected systems. Input filters are added at the front end of these converters to prevent the switching noise from entering the source subsystem. Stringent EMI specifications exist that impose upper bounds on the input filter transfer characteristics at different frequency ranges as dictated by the specific application.

A distinguishing feature of modern aircraft power distribution systems is the regeneration of energy from the flight control actuators to the dc bus during certain operating regimes. The regenerative power occurs as a transient disturbance on the dc bus and results in intolerably large voltage swings on the bus. To include the effect of regenerative power on system characteristics, a load disturbance $i_{od}(t)$, which is represented by a pulse load with duration T_p, is included into the sample system as shown in Fig. 1.

The nominal operating conditions for the sample system are given in Table 1. The goal of the optimization is to design these two subsystems such that 1) each subsystem meets its own performance specifications (to be described in the following sections), 2) the overall system is stable within prescribed stability bounds, 3) the effect of the transient disturbance source $i_{od}(t)$ at the output of the buck

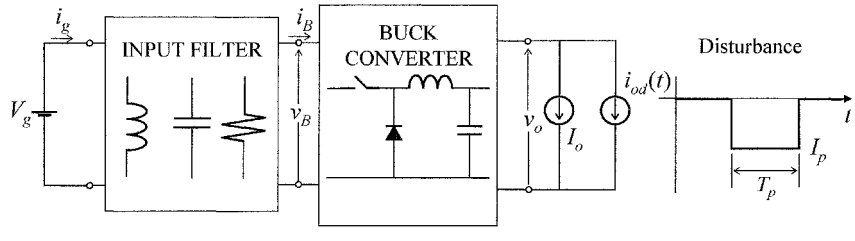

Fig. 1 Block diagram of the sample system.

converter on the input voltage of the converter (i.e., the effect of the regenerative power) is limited, and 4) the overall weight of the system is minimized. In the sections that follow, we will discuss the optimization of each subsystem separately and then the combined optimization of the whole system.

III. Optimized Design of Input Filter

A. Problem Formulation

The filter to be optimized is shown in Fig. 2. It must operate as an integral part of the global system. To account for the interactions with the rest of the system, a voltage source has been added to the input of the filter, and two current sources have been added to the output of the filter. The constant current source accounts for the nominal current load of the buck converter in the sample system discussed in the last section. The time-varying current source accounts for the regenerative energy from the buck converter. This current source represents the dynamic coupling between various blocks of the power distribution system.

The basic design problem is to select the component values of this filter, including the physical parameters of the inductors. To formulate the optimization procedure, it is necessary to 1) develop the model of the filter, 2) identify the design variables, 3) specify the constraints, and 4) define the objective function. Each of these elements of the optimization methodology is discussed in this section.

B. Model, Design Variables, and Objective Function

1. Filter Model

The model for this subsystem can easily be developed using standard network analysis. For the optimization procedure, the model is written in the standard state-space form.

Table 1 Nominal operating conditions for sample system

Variable	Description	Value
V_g	Filter input voltage	270 V
V_B	Filter output voltage	270 V
V_o	Converter output voltage	100 V
D	Converter duty cycle	V_o/V_g
I_o	Converter average load current	15 A
I_B	Converter input current	$I_o(V_o/V_g)$
I_p	Peak value of pulse disturbance	−20 A
T_p	Duration of pulse disturbance	10 ms

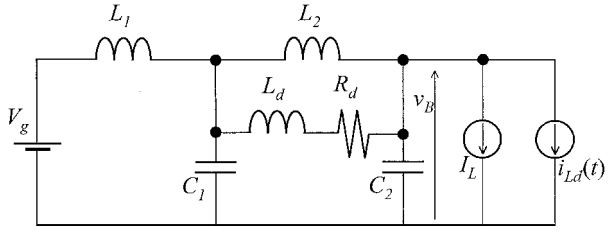

Fig. 2 Schematic of input filter used in sample system.

2. Design Variables

For the input filter shown in Fig. 2, the design variables include the capacitance values C_1 and C_2, resistance value R_d, and the elements of the three inductors. In the present work, the inductor design includes the physical design of the inductor's components, not just the selection of the value of the inductance. The inductors are assumed to use typical EE cores (Fig. 3) that are defined by a set of geometric variables.

The quantities K_1 and K_2 shown in Fig. 3 are assumed to be fixed and represent the aspect ratios of the center leg and the window, respectively. The bobbin is housed on the center leg of the core. The bobbin, along with the windings, is placed around the center leg before the two halves of the EE core of the inductor are fastened together. The inductance as a function of these physical variables is given by

$$L = \mu_o K_1 C_w^2 n^2 / l_g \tag{1}$$

The complete set of input filter design variables is listed in Table 2. Note that these variables include parameters related to the windings and wire size, as well as the geometry variables.

3. Objective Function

The objective function is the weight of the input filter. The total filter weight is the sum of the weights of the inductors, capacitors, and resistors

$$J = W_L + W_C + W_R \tag{2}$$

The weight of an inductor is determined as the sum of the weights of ferrite and copper used in the core and windings, respectively,

$$W_L = W_{\text{Fe}} + W_{\text{Cu}} \tag{3}$$

Table 2 Design variables for the input filter

Design variable	Description
C_1	Filter capacitance
C_2	Filter capacitance
R_d	Filter resistance
n_d	Number of turns for L_d
$A_{\text{cp}d}$	Cross-sectional area of winding for L_d
C_{wd}	Center leg width for L_d
W_{wd}	Window width for L_d
l_{gd}	Airgap length for L_d
n_1	Number of turns for L_1
$A_{\text{cp}1}$	Cross-sectional area of winding for L_1
C_{w1}	Center leg width for L_1
W_{w1}	Window width for L_1
l_{g1}	Airgap length for L_1
n_2	Number of turns for L_2
$A_{\text{cp}2}$	Cross-sectional area of winding for L_2
C_{w2}	Center leg width for L_2
W_{w2}	Window width for L_2
l_{g2}	Airgap length for L_2

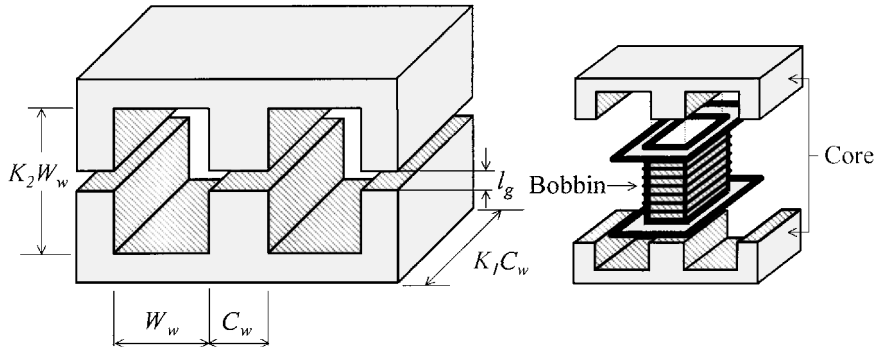

Fig. 3 EE core and relevant dimensions.

From Fig. 3, the weight of the copper can be obtained as

$$W_{\mathrm{Cu}} = \rho_{\mathrm{Cu}} \mathrm{vol}_{\mathrm{Cu}} = \rho_{\mathrm{Cu}} \cdot \mathrm{MLT} \cdot n \cdot A_{\mathrm{cp}} \tag{4}$$

where the mean turn length per turn (MLT) $= 2F_c C_w(1 + K_1)$ and the pitch winding factor is $F_c = 1.9$. Similarly, the weight of the iron used in the EE core is given by (Fig. 3)

$$W_{\mathrm{Fe}} = \rho_{\mathrm{Fe}} \mathrm{vol}_{\mathrm{Fe}} = \rho Z_p A_p = \rho Z_p K_1 C_w^2 \tag{5}$$

where the magnetic path length is

$$Z_p = 2(1 + K_2) W_w + (\pi/2) C_w \tag{6}$$

The weight of a capacitor is approximated as a function of the energy stored in it and is given by

$$W_C = \alpha_C C V_C^2 \tag{7}$$

The constant α_C was empirically obtained from manufacturer data sheets. Finally, the weight of the resistor is approximated as a function of the energy dissipated in it and is given by

$$W_R = \alpha_R \int_0^t R \cdot i_R^2 \cdot \mathrm{d}t \tag{8}$$

C. Constraints

1. *Physical Constraints*

These constraints are defined to guarantee physically meaningful dimensions for the core and windings used in the inductor (Fig. 3). They are defined as follows[2]: 1) The widths of the center leg C_w and of the window W_w are not allowed to be less that 1 mm to ensure sufficient mechanical strength of the core. 2) To ensure sufficient mechanical strength for the winding, the copper wire used can not be greater than 30 AWG (American Wire Gage), which is equivalent to a cross-sectional area of 7.29×10^{-8} m^2. 3) The number of turns in the inductor can not be less than one and must be an integer (this variable is treated as a continuous variable in the gradient-based optimization reported here). 4) The current density in the windings of the inductor can not be greater than the maximum allowable current density for copper. 5) The window of the EE core houses the windings and the bobbin. The area occupied by the windings is given by

$$W_a = n A_{\mathrm{cp}} / F_w \tag{9}$$

where $F_w = 0.4$ is the window fill factor. 6) The window fill factor is included to account for imperfections in the windings on the bobbin. The area occupied by the bobbin in the window, using simple geometry, can be determined as

$$W_b = W_{\mathrm{bob}} K_2 W_w \tag{10}$$

where W_{bob} is the thickness of the bobbin wall. Hence, the window is required to be large enough to accommodate the windings and the bobbin. This requirement is formulated as a constraint given by

$$K_2 W_w^2 > W_a + W_b \tag{11}$$

7) The dimensions of the inductor should be such that the maximum allowable saturation flux density for a ferrite core material, $B_{\mathrm{sp}} = 0.3$ T, is not exceeded to prevent the inductor core from running into saturation. The maximum flux density is determined as the ratio of the maximum flux to the area of cross section of the center leg. Hence, this constraint is given by

$$B_{\mathrm{sp}} > \frac{\Phi_{\mathrm{pk}}}{A_{Cw}} = \frac{(\psi_{\mathrm{pk}}/n)}{K_1 C_w^2} = \frac{(L I_{L(\mathrm{pk})}/n)}{K_1 C_w^2} \tag{12}$$

2. *Performance Constraints*

Performance constraints are further classified as frequency-domain and time-domain constraints.

a. Frequency-domain constraints. As mentioned earlier, input filters are added at the front end of switching converters to prevent the high-frequency noise from entering the source subsystem. Stringent EMI specifications exist that impose upper bounds on the input filter transfer characteristics at different frequency ranges, as dictated by the specific application. The EMI specifications on the input filter are typically translated into frequency domain constraints on the forward voltage transfer function of the input filter. This transfer function between the input and output voltage of the input filter in Fig. 2 is given by

$$V_B(j\omega)/V_g(j\omega) = A_v(j\omega) \tag{13}$$

The frequency response of the forward voltage transfer function for a typical input filter is shown in Fig. 4.

Two types of constraints exist for the frequency-response function: low-frequency passband constraints and high-frequency stopband constraints. The transfer of power from the source to the load occurs almost entirely in the low-frequency region. Hence, the input filter needs to be designed to have a near-unity gain in this region, called the passband. These passband constraints are defined in terms of upper and lower bounds on the input–output transfer function of the filter, up to a passband edge frequency ω_p, as shown in Fig. 4. For the present problem, the passband constraint is defined as

$$-1 \text{ dB} \le |A_v(j\omega)| \le 6 \text{ dB} \tag{14}$$

for $0 \le \omega \le \omega_p = 2\pi 5 \times 10^3$ rad/s.

In addition, the filter must attenuate the high-frequency switching noise according to given EMI specifications. When this filter is attached to a switching power converter, the EMI specifications are often defined by the switching frequency of the converter,[6] here assumed to be 100 kHz. For the present problem, the stopband constraint is

$$|A_v(j\omega)| < -60 \text{ dB} \tag{15}$$

for $\omega > \omega_{s1} = 2\pi \cdot 50 \times 10^3$ rad/s.

b. Time-domain constraints. The time-domain constraints account for the dynamic coupling between the various components of the power distribution system. In the sample system shown in Fig. 1, a pulse current load at the output of the buck converter develops a transient current disturbance $i_{Bd}(t)$. This transient current represents the regenerative energy from the actuator. This transient current will cause an undesirable voltage swing at the output of the filter. A time-domain constraint on the output voltage is imposed to limit the effect of the disturbance. This constraint is an upper bound on the maximum transient excursion of the output voltage of the filter as indicated in Fig. 5. For the present work, the maximum transient voltage excursion limit is $\Delta v_B < 20$ V.

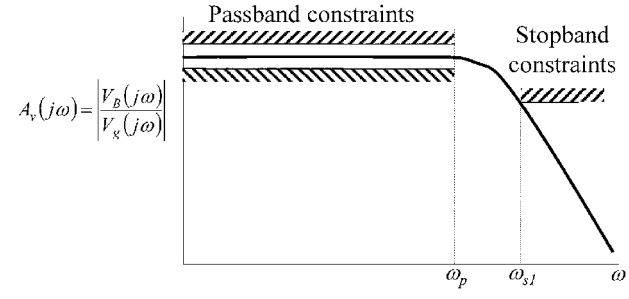

Fig. 4 Frequency-domain performance specifications for the input filter, where $A_v(j\omega) = |v_B(j\omega)/V_g(j\omega)|$.

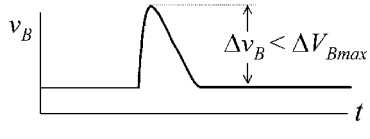

Fig. 5 Constraint for output voltage of the input filter.

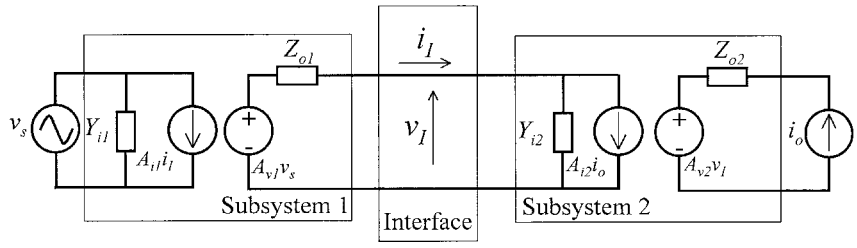

Fig. 6 Generic subsystem interface.

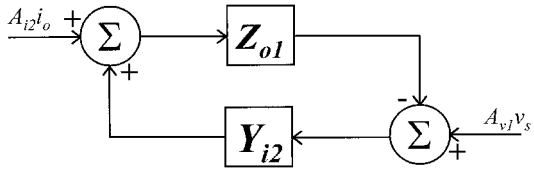

Fig. 7 Feedback loop at the interface due to interconnection of subsystems 1 and 2.

3. Stability Constraints

Because the input filter consists only of passive components, it is generally internally stable. However, the input filter is notorious for causing instability due to its interaction with a regulated converter. It can be shown that a regulated power converter can have a negative input impedance that might cause the interconnected system to become unstable. Constraints that guarantee stability of the interconnected system are defined in the frequency domain using the Middlebrook impedance ratio criterion.[7] The impedance ratio criterion is briefly explained in the following.

Suppose we have two interconnected electrical subsystems, as in our sample system. Let each subsystem be represented by a standard two-port model as shown in Fig. 6. The current i_I and voltage v_I at the interface are given by

$$i_I = A_{i2}i_o + Y_{i2}v_I, \qquad v_I = A_{v1}v_s - Z_{o1}i_I \tag{16}$$

From Eq. (16), it can be seen that the interconnection results in a feedback loop, as shown in Fig. 7.

The stability of the interconnected system depends on the stability of the feedback loop. The sufficient condition for the stability of the feedback loop and, hence, of the interconnected system is given by the small-gain theorem. Applied here, we have

$$\|Z_{o1}(j\omega)\| \cdot \|Y_{i2}(j\omega)\| \ll 1 \tag{17}$$

This expression can be rewritten as

$$\|Z_{o1}(j\omega)\| \ll 1/\|Y_{i2}(j\omega)\| = \|Z_{i2}(j\omega)\| \tag{18}$$

which implies that the magnitude of the output impedance of subsystem 1 (filter) must everywhere be less than the input impedance of subsystem 2 (converter). Equation (18) is traditionally known as the impedance ratio criterion.

Now we apply this idea to our filter design problem. Of course, the stability criteria must be applied twice: once to the interaction with the buck converter at the output of the filter and once to the interaction with the voltage bus at the input to the filter. The input filter schematic showing only the relevant impedances is shown in Fig. 8.

Consider first the output of the filter. The impedance looking out of the output terminals of the filter is designated Z_{iL}, and it is the input impedance of the buck converter. For the filter optimization problem, this impedance is considered to be fixed and given. The impedance Z_{of} is the impedance looking into the output terminals of the filter. It is calculated from the design model and depends on the design variables of the input filter. When the impedance ratio criteria are applied, the output impedance of the filter Z_{of}, which depends on the design parameters, must be less than the impedance

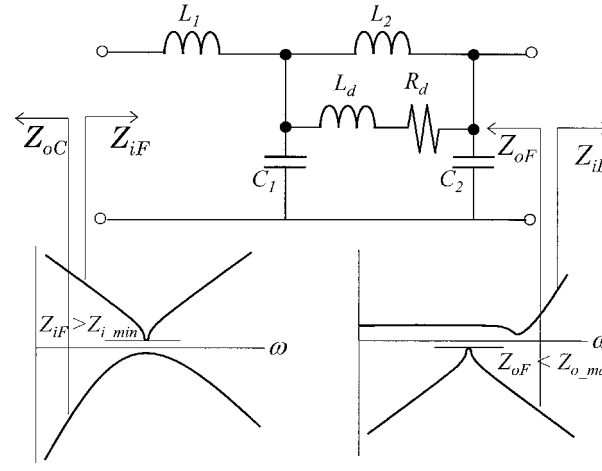

Fig. 8 Impedances at the terminals of the input filter.

Z_{iL}. Because Z_{iL} is given, sufficient separation between these two impedances can be enforced by requiring that the upper bound of the output impedance of the filter satisfy

$$Z_{o\_\max} = \max_{\omega}[|Z_{oF}(j\omega)|] < 15 \text{ dB} < Z_{iL} \tag{19}$$

A similar reasoning is applied to the interaction between the filter and the power bus. When the impedance ratio criteria is applied, we obtain the constraint

$$Z_{i\_\min} = \min_{\omega}[|Z_{iF}(j\omega)|] > 3 \text{ dB} > Z_{oC} \tag{20}$$

D. Optimization Results

Optimization was performed using a commercially available program, VisualDOC optimization software.[8] The modified method of feasible directions algorithm[9] was utilized. The transient peak voltage constraint was enforced by imposing an upper bound constraint on the maximum output voltage obtained from a time domain simulation of the filter response. The input impedance constraint was enforced by imposing a lower-bound constraint on the minimum input impedance obtained from a frequency domain simulation of the filter response. Likewise, the output impedance constraint was enforced by imposing an upper-bound constraint on the maximum output impedance obtained. Constraint derivatives were computed using finite differences. Depending on the initial design used to start the optimization iterations, convergence was obtained within approximately 200 function evaluations. (Here, a single function evaluation includes both a time-domain simulation and frequency-domain computations.) The optimizations were achieved in approximately 40 min on a 500-MHz Pentium III personal computer.

To assess the validity of the results obtained from the optimizer, the optimal designs were compared to a filter built for a three-phase buck converter for a telecommunications application.[5] This hardware design, developed without the use of the optimizer, is referred to here as the nominal design.

Because the optimization algorithm is a gradient-based method, the initial design point may be trapped by a local minimum. In the present work, it was found that there were local minima in the design

Table 3 Physical variables of the filter inductors

Variable	Nominal value	Optimal value
n_1	29.53	19.94
A_{cp1}	0.630×10^{-5} m^2	0.530×10^{-5} m^2
C_{w1}	0.751×10^{-2} m	0.484×10^{-2} m
W_{w1}	0.682×10^{-2} m	1.017×10^{-2} m
l_{g1}	1.16×10^{-3} m	0.664×10^{-3} m
n_2	45.98	42.77
A_{cp2}	0.448×10^{-5} m^2	0.382×10^{-5} m^2
C_{w2}	0.985×10^{-2} m	0.939×10^{-2} m
W_{w2}	1.33×10^{-2} m	1.244×10^{-2} m
l_{g2}	1.29×10^{-3} m	1.03×10^{-3} m
n_d	16.06	7.79
A_{cpd}	0.349×10^{-5} m^2	0.359×10^{-5} m^2
C_{wd}	0.396×10^{-2} m	0.585×10^{-2} m
W_{wd}	0.978×10^{-2} m	0.564×10^{-2} m
l_{gd}	0.355×10^{-3} m	0.176×10^{-3} m

Table 4 Nominal and optimal filter designs

Variable	Nominal value	Optimal value
L_1, μH	80	26.49
L_2, μH	300	296.77
L_d, μH	21.5	22.29
C_1, μF	5	7.19
C_2, μF	18.8	27.70
R_d, Ω	3	2.23
Weight, kg	0.5279	0.3692

Table 5 Response quantities for nominal and optimal designs of input filter

Response variable	Nominal	Optimal
Minimum input impedance, dB	3.81[a]	**2.99**
Maximum output impedance, dB	15.39	9.11
Passband maximum, dB	5.63	3.18
Passband minimum, dB	6.55×10^{-6}	7.94390×10^{-6}
Stopband maximum, dB	−63.13	**−60.00**
Peak output voltage, V	21.97[a]	13.75

[a]Violated constraint.

space, although in all cases studied even the local minima were lighter than the nominal design. The results reported here correspond to the best designs found during the course of the study and are likely to be the globally optimum design.

The physical variables for the filter inductors values for the nominal and optimal designs are given in Table 3. The nominal and optimum component values and the objective function are provided in Table 4. Response quantities of interest for the nominal and optimal designs are given in Table 5. Response quantities that are at their upper or lower bounds are listed in boldface type. The physical constraints on the current density, available window area, and saturation flux density for each of the three inductors were active for the optimal design. The other active constraints for the optimized design were the lower-bound constraint on the input impedance Z_{iF} and the stopband constraint on the input–output transfer function. Note that the peak voltage constraint was violated for the nominal design.

To compare the optimization results with the hardware (nominal) design, several additional optimization runs were performed corresponding to different values of the lower-bound constraint $Z_{i\_\min}$ on the input impedance. The resulting family of optimal designs is compared to the nominal design in Fig. 9. For the same value (3.8 dB) of $Z_{i\_\min}$, the optimal design is 25% lighter than the nominal design. For the same weight, on the other hand, the minimum input impedance for the optimized design is approximately 47% higher than for the nominal design. In addition to providing weight savings in comparison to the nominal design, the optimal design methodology is automated and considerably reduces the design cycle time.

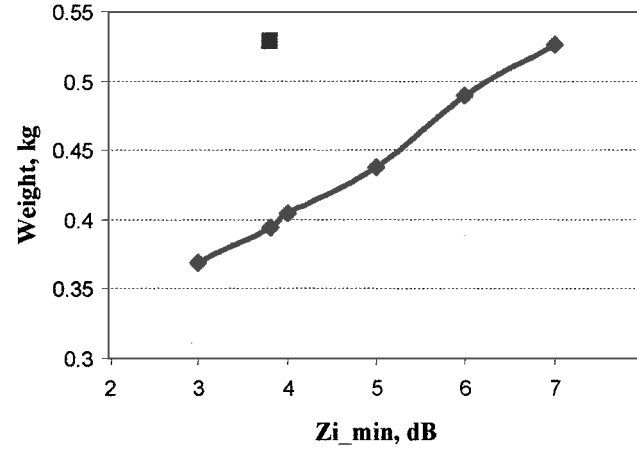

Fig. 9 Weight of optimal designs as a function of the lower bound on the input impedance.

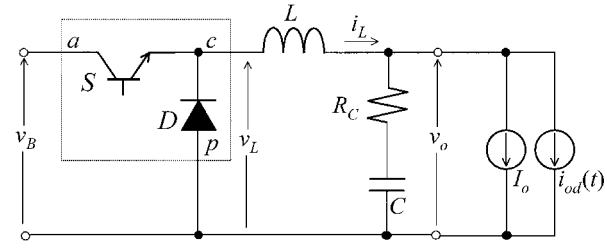

Fig. 10 Schematic of dc–dc buck converter.

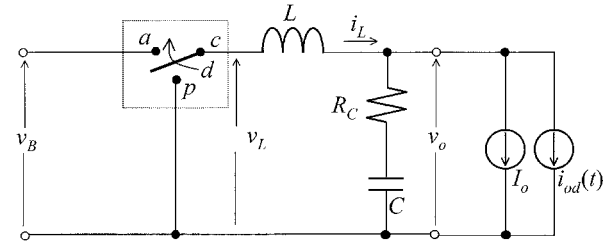

Fig. 11 Realization with PWM switch.

IV. Optimized Design of Buck Converter

A. Buck Converter Model, Design Variables, and Objective Function

Next, we consider the formulation of the optimization problem for the design of the buck converter, the second subsystem in the sample system discussed in Sec. II. The approach to this subsystem is very similar to the approach taken for the filter, particularly the interaction constraints. Some additional constraints are required for the converter, however, because of its internal complexity.

1. Buck Converter Model

The schematic of the dc–dc buck converter is shown in Fig. 10. The switch–diode combination highlighted in Fig. 10 is replaced by a single-pole double-throw switch, known as the PWM (pulse width modulated) switch, as shown in Fig. 11. The switch S is turned on (switch at position a in Fig. 11) and off (switch at position b in Fig. 11) at a fixed frequency to transform the input voltage v_B to a periodic square wave voltage v_L. The voltage v_L is then filtered by the L–C filter to obtain the output voltage v_o. The average value of the output voltage is varied by modulating the time interval the switch S is kept on. The fraction of the time period T for which the switch is kept on is known as the duty cycle d of the switch. The values of L and C and the switching frequency f_s determine the switching ripple in the inductor current i_L and output voltage v_o. Approximate waveforms of the inductor current and the output voltage, including the switching ripple, are shown in Fig. 12. To regulate tightly the average value of the output voltage to a fixed reference, a feedback compensator is used to control the duty cycle d of the switch against disturbances in the load current i_o and input voltage v_B.

Table 6 Design variables for buck converter

Design variable	Description
n	Number of turns for L
A_{cp}	CSA of winding for L
C_w	Center leg width for L
W_w	Window width for L
l_g	Airgap length for L
C	Capacitance
f_s	Switching frequency of buck converter
h_o	Voltage controller gain
ω_z	Voltage controller zero
ω_p	Voltage controller pole
h_{ip}	Current controller proportional gain
h_{ii}	Current controller integral gain

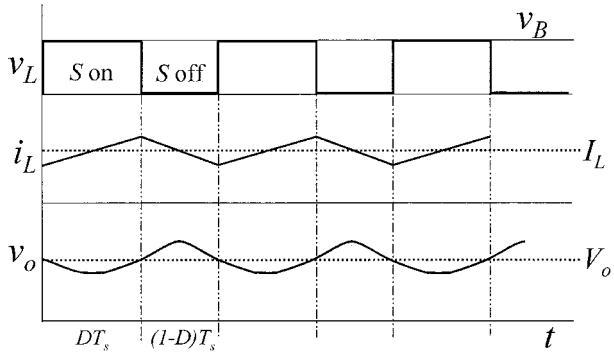

Fig. 12 Switching waveforms of inductor current and output voltage.

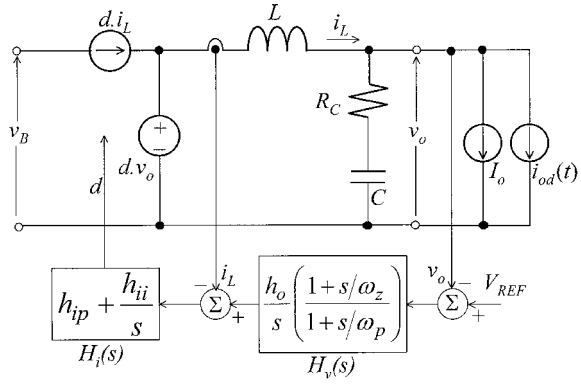

Fig. 13 Average model of buck converter.

In this paper, an average model of the buck converter, which neglects the switching ripple in the currents and voltages, is used.[6] The average model of the buck converter replaces the switch–diode combination in the switch model (a in Fig. 10) by controlled current and voltage sources. A multiloop controller consisting of an inner inductor current loop and an outer voltage loop is used for the regulation of the output voltage to a fixed reference. The average model of the buck converter along with a block diagram of the controller is shown in Fig. 13. The model of the buck converter can now be derived from Fig. 13 using standard circuit analysis techniques.

2. Design Variables

Design variables for the buck converter include the physical parameters governing the design of the inductor L, the capacitance C, the switching frequency of the converter f_s, and a set of parameters governing the feedback controller (h_o, ω_z, ω_p, h_{ip}, and h_{ii}). As with the filter, it is assumed that an EE core is used for the inductor (Fig. 3). Table 6 contains a list of all design variables used for the buck converter.

3. Objective Function

The objective function is the weight of the inductor and capacitor, which is calculated according to Eq. (2) as the sum of the weights of the inductors and the capacitors. The controller is not assumed to contribute significantly to the weight of the converter and, hence, is neglected in the determination of the weight. In addition, because thermal considerations were not included in the optimization formulation, the weight of the heat sink was excluded from the objective function.

B. Constraints

The performance, stability, and physical constraints on the design of the buck converter are described in the following paragraphs.

1. Performance Constraints

The performance constraints consist of both time and frequency domain constraints.

a. Frequency-domain constraints. Two frequency-domain constraints are imposed on the buck converter. In Fig. 13, the transfer function between the input voltage v_B and the output voltage v_o is called the audiosusceptibility of the converter. A typical transfer function is shown in Fig. 14. An upper bound is imposed on this transfer function to guarantee sufficient rejection of any high-frequency disturbance introduced at the input voltage. This constraint can be stated as

$$A_v = \max_{\omega} |V_o(j\omega)/V_B(j\omega)| < -30\ \text{dB} \tag{21}$$

The second constraint is imposed on the loop gain shown in Fig. 15. The loop gain is the open-loop transfer function in Fig. 13

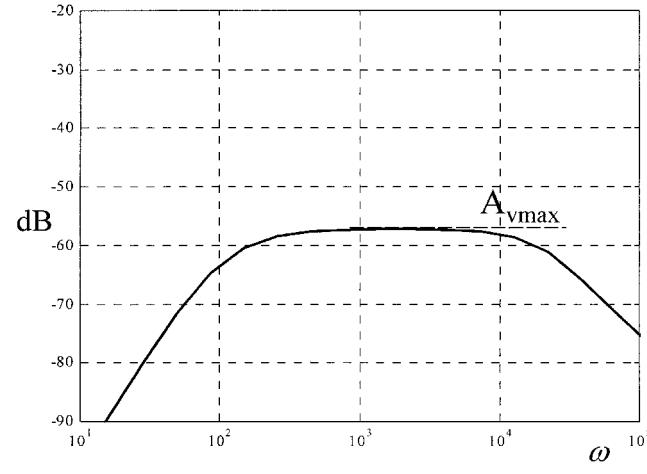

Fig. 14 Frequency-domain constraints on the audiosusceptibility.

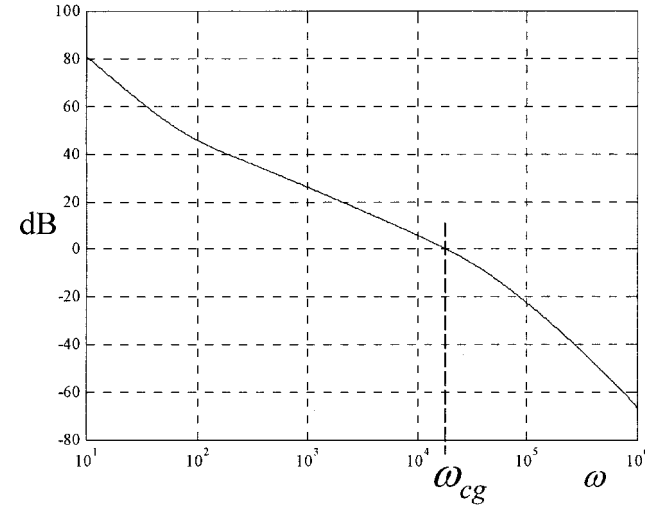

Fig. 15 Frequency-domain constraints on the loop gain.

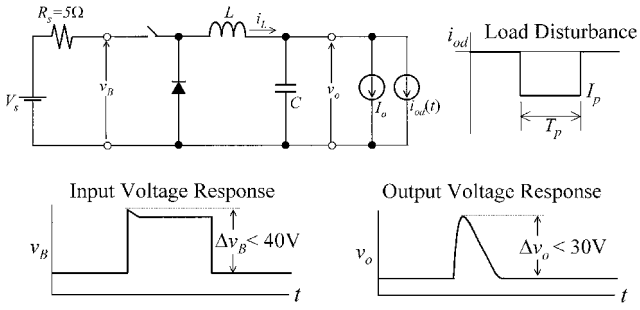

Fig. 16 Time-domain constraints for the converter.

between the output voltage error $V_{\text{ref}} - v_o$, and the output voltage v_o. The characteristics of the loop gain transfer function determine the bandwidth and the stability margins of the closed-loop system. An upper-bound constraint is also imposed on the crossover frequency of the voltage loop gain ω_{cg} to limit the bandwidth of the converter. (This relationship can be found in classical control theory.[10]) The bound on the bandwidth of the converter will guarantee that the switching frequency ripple in the inductor current and the output voltage are sufficiently attenuated before they propagate through the controller. The frequency ω_{cg} is chosen to be sufficiently less than one-half of the switching frequency. For the present problem, this upper bound is given by

$$\omega_{\text{cg}} < 2\pi f_s/5 \tag{22}$$

Additional constraints will be imposed on the voltage loop gain for stability reasons, as will be discussed.

b. Time-domain constraints. Time-domain constraints are introduced to account for transients in the voltages in the converter due to transient disturbances at the output terminals of the converter. These constraints are identical to those developed for the filter in Sec. III. A pulse load disturbance represents the transient disturbance at the output of the buck converter. For the optimized design of the buck converter, a fixed resistance is included in series with an ideal voltage source as shown in Fig. 16.

This fixed resistance was included to represent the effect of the input filter when we impose the impedance ratio criteria for stability. The resistance value was chosen to be equal to 5Ω, which was the maximum output impedance (15 dB) of the nominal input filter design, and the voltage variations at the input and output of the converter were constrained as

$$\Delta v_B < 40 \text{ V}, \qquad \Delta v_o < 30 \text{ V} \tag{23}$$

2. Stability Constraints

Like the filter, the buck converter must satisfy external stability constraints, so that the entire sample system in Fig. 1 is stable. In addition, because of the presence of the internal control loop, the converter must be internally stable.

a. Internal stability constraints. The design of the feedback controller for the buck converter (Fig. 13) must guarantee stability and robustness of the closed-loop system in the presence of disturbances in the load current and source voltage. These stability constraints are defined as bounds on the gain margin g_m and phase margin ϕ_m of the closed loop. From classical control theory,[10] positive values of phase margin and gain margin are necessary conditions for stability. To guarantee sufficient robustness of the closed loop, lower bounds are imposed on these values as

$$\phi_m > 60 \text{ deg}, \qquad g_m > 3 \text{ dB} \tag{24}$$

These values are widely used in the design of switching converters. These constraints translate into constraints on the voltage loop gain in Fig. 14.

b. External stability constraints. External stability constraints are used to guarantee stability of the interconnected system after adding the input filter. As for the input filter, they are defined using the impedance ratio criterion with the input and output impedances appropriately defined. An upper bound is imposed on the maximum magnitude of the output impedance $Z_{o\_\max}$ and a lower bound on the minimum magnitude of the input impedance $Z_{i\_\min}$ of the closed-loop converter. Using the notation of Sec. III, we have

$$Z_{i\_\min} = \min_{\omega}[|Z_{iB}(j\omega)|] > 30 \text{ dB}$$

$$Z_{o\_\max} = \max_{\omega}[|Z_{oB}(j\omega)|] < 20 \text{ dB} \tag{25}$$

Because the output impedance of the filter is set to 15 dB in Eq. (19), the first of these two constraints ensures that there is at least a 15-dB separation between the output impedance of the filter and the input impedance of the converter (Fig. 8.) The upper bound of the output impedance is set to ensure sufficient separation from the minimum input impedance of the load to the buck converter. Because the load is represented by an ideal current source (which has an infinite input impedance), the upper bound of the output impedance was arbitrarily chosen.

3. Additional Constraints

In addition to the physical constraints, which guarantee physically meaningful dimensions for the core and winding of the inductors similar to the input filter, constraints are also imposed to limit the switching ripple in the inductor currents and the capacitor voltages. Although the average model for the buck converter is used for the analysis, expressions for the switching ripple in terms of average quantities are readily available.

a. Inductor current ripple. It is generally required that the peak-to-peak inductor current ripple be less than 10% of the nominal inductor current. From Fig. 12, the inductor current ripple can be obtained as[3]

$$\Delta I_L = [(1 - D)/f_s](V_o/L) \tag{26}$$

If $P_o = V_o I_{L(\text{nom})}$ is the nominal power rating of the converter, a lower bound on the inductance, such that the switching ripple is less than 10% of the nominal inductor current, is then determined as

$$L > 10\left(V_o^2 \big/ P_o\right)(1 - D)/f_s \tag{27}$$

b. Output voltage ripple. The ripple in the output voltage is generally limited to be less than 1% of the average value of the capacitor voltage ripple. It is assumed that the capacitor absorbs the ripple component of the inductor current. The peak-to-peak output voltage ripple constraint is derived as follows[3]:

$$\Delta V_o = (1/8C)(\Delta I_L/f_s) + \Delta I_L R_C \tag{28}$$

When the inductor current ripple from Eq. (27) is substituted for, the output voltage ripple constraint is

$$\Delta V_o = (1/8LC)[(1 - D)/f_s]V_o + [(1 - D)/Lf_s]V_o R_C$$

$$= (1/LC)\left[(1 - D)\big/ f_s^2\right]V_o\left(\tfrac{1}{8} + R_C C f_s\right) < 0.01 V_o \tag{29}$$

If the voltage ripple is constrained to be less than 1% of the average value, then we arrive at the constraint

$$LC > 100 \cdot \left(1 - D\big/ f_s^2\right)\left(\tfrac{1}{8} + R_C C f_s\right) \tag{30}$$

C. Optimization Results

The optimization scheme was same as the input filter optimization discussed earlier. The transient peak voltage constraint was enforced by imposing an upper-bound constraint on the maximum output voltage obtained from a time-domain simulation of the filter response. Converged optimal designs were obtained in approximately 300

Table 7 Physical variables for the inductor in the buck converter

Variable	Nominal value	Optimal value
n	55	55.55
A_{cp}, m^2	1.1×10^{-5}	1.05×10^{-5}
C_w, m	1.65×10^{-2}	1.626×10^{-2}
W_w, m	2.5×10^{-2}	2.28×10^{-2}
l_g, m	3.9×10^{-3}	3.66×10^{-3}

Table 8 Component values and objective function for the buck converter

Variable	Nominal value	Optimal value
L, μH	**400**	**419.75**
C, μF	82	46.88
h_o	1	0.881
ω_z, rad/s	100	420.14
ω_p, rad/s	40000	54983
h_{ip}	1	0.998
h_{ii}	100	100
f_s, kHz	100	100
Weight, kg	**1.5637**	**1.5072**

Table 9 Response quantities for nominal and optimal designs

Response variable	Nominal	Optimal
Inductor current ripple, A	1.574[a]	**1.5**
Capacitor voltage ripple, V	0.6	**1**
Phase margin, deg	72.5	69.54
Gain margin, dB	58.67	37.13
Minimum input impedance, dB	33.72	33.69
Maximum output impedance, dB	0.02	1.25
Audiosusceptibility, dB	−57.24	−55.99
Peak output voltage, V	19.85	22.61
Peak input voltage, V	37.38	38.85

[a]Violated constraint.

function evaluations. (A single function evaluation includes both a time-domain simulation and frequency-domain computations.) The optimizations were achieved in approximately 20 min on a 500-MHz Pentium III personal computer. The optimal design for the buck converter was generally insensitive to the initial design.

The physical variables for the filter are given in Table 7, and the nominal and optimal designs of the buck converter, along with the corresponding objective functions, are presented in Table 8. Response variables of interest for the optimized buck converter are given in Table 9. Response variables at their upper or lower bounds are listed in boldface type. The active constraints for the optimized converter design were the physical constraints on the design of the inductor and the constraint on the input voltage variation to the transient load disturbance.

The optimized converter design is not significantly lighter than the nominal design, but it was obtained in a shorter period of time and with a minimal amount of effort compared to the standard manual design procedures.

V. Optimization of Coupled System

A. Formulation of the Combined Optimization

The optimization problems for the input filter and buck converter were specifically formulated to allow them to be integrated into a combined optimization with minimal modifications. The design variables are those of the input filter and the converter as shown in Tables 2 and 6. The constraints on the optimization of the interconnected system are obtained from those of the designs of each of the individual systems, with some modifications to account for interactions between the input filter and the converter. The constraints that need to be modified are those that are defined at the interface between the input filter and the converter.

1) Because of the interconnection of the filter and the converter, it may not be appropriate to impose fixed limits on the output

Table 10 Physical variables of inductors in sample system

Variables	Nominal	Individual optimization	Integrated optimization
		Filter	
n_1	29.53	19.94	20.01
A_{cp1}, m^2	0.630×10^{-5}	0.530×10^{-5}	0.521×10^{-5}
C_{w1}, m	0.751×10^{-2}	0.484×10^{-2}	0.480×10^{-2}
W_{w1}, m	0.682×10^{-2}	1.017×10^{-2}	1.014×10^{-2}
l_{g1}, m	1.16×10^{-3}	0.664×10^{-3}	0.657×10^{-3}
n_2	45.98	42.77	42.81
A_{cp2}, m^2	0.448×10^{-5}	0.382×10^{-5}	0.370×10^{-5}
C_{w2}, m	0.985×10^{-2}	0.939×10^{-2}	0.914×10^{-2}
W_{w2}, m	1.33×10^{-2}	1.244×10^{-2}	1.230×10^{-2}
l_{g2}, m	1.29×10^{-3}	1.03×10^{-3}	1.017×10^{-3}
n_d	16.06	7.79	7.78
A_{cpd}, m^2	0.349×10^{-5}	0.359×10^{-5}	0.356×10^{-5}
C_{wd}, m	0.396×10^{-2}	0.585×10^{-2}	0.576×10^{-2}
W_{wd}, m	0.978×10^{-2}	0.564×10^{-2}	0.561×10^{-2}
l_{gd}, m	0.355×10^{-3}	0.176×10^{-3}	0.172×10^{-3}
		Buck converter	
n	55	55.55	55.55
A_{cp}, m^2	1.1×10^{-5}	1.05×10^{-5}	1.05×10^{-5}
C_w, m	1.65×10^{-2}	1.626×10^{-2}	1.63×10^{-2}
W_w, m	2.5×10^{-2}	2.28×10^{-2}	2.28×10^{-2}
l_g, m	3.9×10^{-3}	3.66×10^{-3}	3.67×10^{-3}

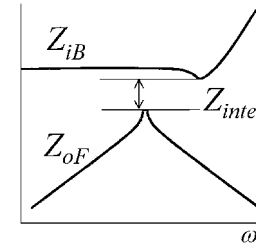

Fig. 17 Interaction constraints on the sample system design.

impedance of the filter and the input impedance of the converter, as was the case when they were designed independently. Because a sufficient condition for stability is to ensure a minimum separation between the two impedances, the constraints on the minimum input impedance of the converter Z_{iB} and the maximum output impedance of the filter Z_{oF} are replaced by a single constraint that imposes a lower bound on the difference between the two, as shown in Fig. 17. The interaction constraints used for the current example are

$$\min_{\omega}[|Z_{iB}(j\omega)|] - \max_{\omega}[|Z_{oF}(j\omega)|] > 15 \text{ dB} \tag{31}$$

The 15-dB separation used in the first constraint is consistent with the constraints used for the individually optimized designs (19) and (25) presented earlier. All other constraints are directly carried over from the optimization formulations of the input filter and the buck converter.

2) The constraint on the transient excursions on the output voltage of the input filter and the input voltage of the converter are replaced by a single constraint on the maximum excursion of the interface voltage v_B, $v_B < 20$ V.

3) The objective function is the total weight of the input filter and converter.

B. Optimization Results

Converged optimal designs were obtained in approximately 1400 function evaluations, where a single function evaluation again includes both a time-domain simulation and frequency-domain computations. The optimizations were achieved in approximately 90 min on a 500-MHz Pentium III personal computer.

The physical variables associated with the inductors in the sample system are given in Table 10. Component values and objective functions are given in Table 11. The important responses are listed in Table 12. The active constraints for the filter in this optimization run were all of the physical constraints on the design of the

inductors, the lower-bound constraint on the input impedance, the upper-bound stopband constraint, and the upper-bound constraint on the passband. The active constraints on the converter were the physical constraints on the inductor design and the upper bound on the voltage variation at the output due to a load disturbance.

The filter design obtained from the combined problem is 5% lighter than that obtained from the individual optimization, whereas the converter design obtained for the combined optimization problem is almost identical to that obtained independently. Differences in the combined designs and the independently obtained designs arise because the interconnection of two subsystems creates a feedback loop where a change in the source subsystem causes a change in the load subsystem and vice versa. When the optimization was performed on the integrated sample system as a whole, the optimizer was able to take advantage of the interaction between the filter and converter and reduce the overall system weight.

When the input filter was optimized individually, the load disturbance was represented by a pulse current load similar to that at the output of the converter, except that it was scaled by its duty

Table 11 Component values and objective function for the sample system

Variables	Nominal	Individual optimization	Integrated optimization
		Filter	
L_1, μH	80	26.49	26.531
L_2, μH	300	296.77	283.84
L_d, μH	21.5	22.29	22.045
C_1, μF	5	7.19	7.21
C_2, μF	18.8	27.70	27.86
R_d, Ω	3	2.23	2.27
Weight, kg	**0.5279**	**0.3692**	**0.3495**
		Buck converter	
L, μH	400	419.75	419.75
C, μF	82	46.88	46.904
h_o	1	0.881	0.880
ω_z, rad/s	100	420.14	420.12
ω_p, rad/s	40000	54983	54998.2
h_{ip}	1	0.998	0.998
h_{ii}	100	100	100
f_s, kHz	100	100	100
Weight, kg	**1.5637**	**1.5072**	**1.5072**

Table 12 Response quantities of integrated optimization

Response quantity	Value
Input filter	
Minimum input impedance	**3.00** dB
Maximum output impedance	9.3382 dB[a]
Passband maximum	3.36 dB
Passband minimum	4.87×10^{-6} dB
Stopband maximum	-60 dB
Buck converter	
Phase margin	69.57°
Gain margin	37.18 dB
Minimum input impedance	33.72 dB[a]
Maximum output impedance	1.25 dB
Audiosusceptibility	-55.98 dB
Peak output voltage	22.59 V
Interface quantities	
Impedance difference	24.378 dB
Peak interface voltage	11.81 V

[a]These responses were not constrained while performing the integrated optimization. They are shown here for the sake of completeness.

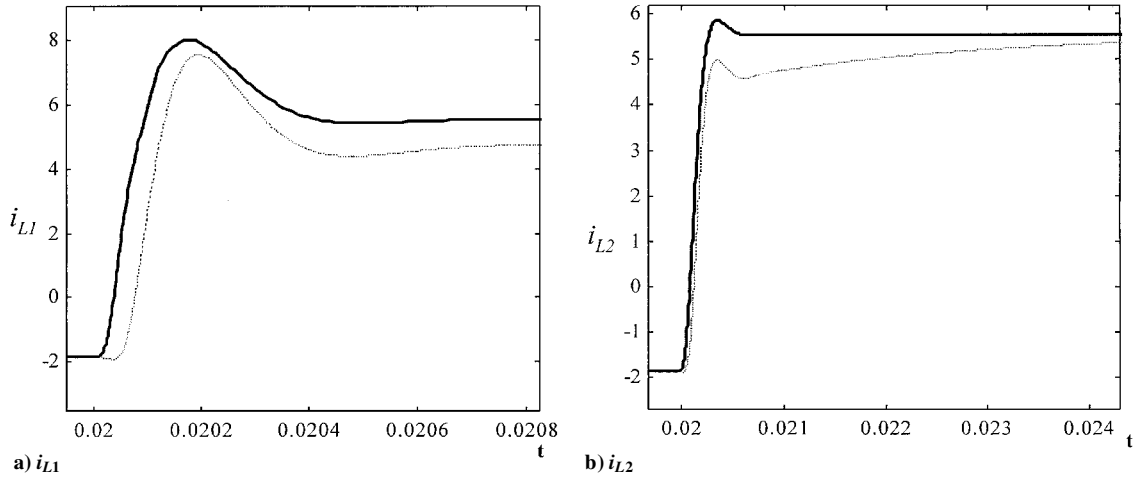

Fig. 18 Filter inductor currents with (– – –) and without (——) buck converter.

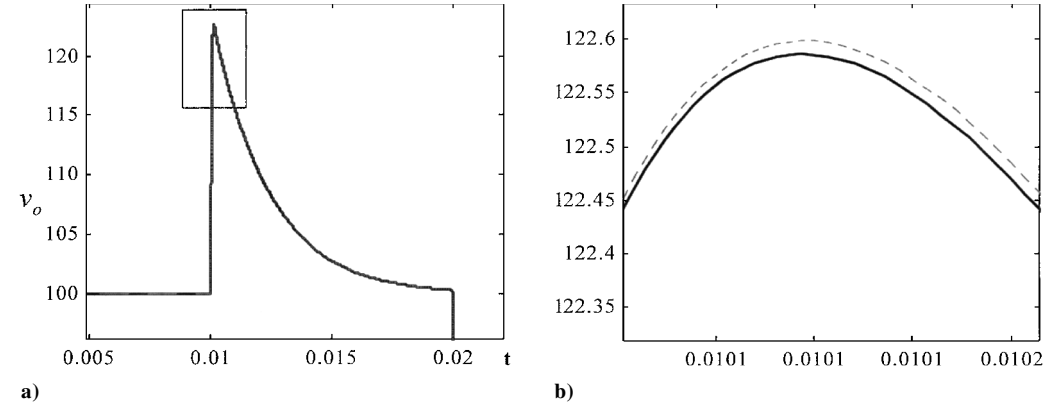

Fig. 19 Converter output voltage in sample system with individually optimized converter design (——) and converter design obtained from optimized sample system (– – –) (b) is enlargement of the peak in (a).

cycle. When the converter and the filter are optimized together, the load disturbance at the output of the filter (and, hence, at the input of the converter) is filtered by the presence of the converter. Hence, the transient peak currents flowing into the inductors of the filter are less than those that were present when the filter was optimized individually. This is illustrated in Fig. 18, where the transient responses of the filter inductor current i_{L1}, with and without the buck converter, are shown. Because the peak currents flowing into the filter inductors are lower when the converter is taken into account, smaller inductors can be used. This results in a lower weight filter.

Simulation results of the sample system with the converter design obtained from the individual and integrated optimizations are shown in Fig. 19. It can be seen from Fig. 19 that the output voltage variation of the buck converter in the optimized sample system is higher than that of the individually optimized converter. The optimizer increases the capacitance slightly (Table 9) at the output of the buck converter to allow a larger voltage variation. This change allows a larger portion of the transient current to flow into the output capacitance of the buck converter than propagate to the filter. This enables the filter weight to be decreased. The optimizer was, therefore, able to take advantage of the system interactions and the more accurate representations of the load disturbances and voltage variations to arrive at an improved (lower weight) design for the combined filter/converter sample system.

VI. Conclusions

In this paper, we considered the problem of formulating a mathematical optimization problem for the weight minimization of an aircraft power distribution system. The approach is to develop a mathematical optimization problem for the various components of the power distribution system in such a way that these component problems can be easily integrated into a larger optimization problem. This concept is demonstrated on a simple interconnected system consisting of an input filter and a regulated dc–dc buck converter. First, an optimization problem is developed for the filter and the converter separately, and it is shown that reasonable results are obtained. Next, an optimization problem is developed for the interconnected system using the optimization formulations of the two subsystems. It was shown that optimizing the sample system as a whole resulted in a lesser weight because the optimizer was able to account for the interactions between the interconnected subsystems.

The use of optimization methodologies may potentially allow designers to obtain minimum weight designs in a much shorter design cycle time than is required using traditional design techniques.

Acknowledgments

The research reported in this paper is supported by the U.S. Air Force Office of Scientific Research under Grants F49620-97-1-0254 and F49620-99-1-0104 and made use of Engineering Research Center (ERC) Shared Facilities supported by the National Science Foundation under Award Number EEC-9731677.

References

[1]Ragon, S. A., Chandrasekaran, S., Gürdal, Z., and Lindner, D. K., "Optimal Design of a Power Distribution Subsystem," AIAA Paper 2000-0564, *Proceedings of the 38th Aerospace Sciences Meeting and Exhibit*, Reno, NV, Jan. 2000.

[2]Ridley, R. B., Zhou, C., and Lee, F. C., "Application of Nonlinear Design Optimization for Power Converter Components," *IEEE Transactions on Power Electronics*, Vol. 5. No. 1, 1990, pp. 29–39.

[3]Kragh, H., Blaabjerg, F., and Pederson, J., "An Advanced Tool for Optimized Design of Power Electronic Circuits," *Conference Record of the 1998 IEEE Industry Applications Conference*, Vol. 1, IEEE Publ., Piscataway, NJ, 1998, pp. 991–998.

[4]Hopkins, D. C., Sarkar, M., and Cull, R., "A Mathematical Approach to Minimize the Total Mass of a Space Based Power System by Using Multivariate Non-Linear Optimization," *Proceedings of the 29th Intersociety Energy Conversion Engineering Conference*, Vol. 1, 1994, pp. 185–189.

[5]Wang, K., Chandrasekaran, S., Cuadros, C., Dubovsky, S., Torvund, T., Yan, X., Tang, Y., Wang, Y., Boroyevich, D., and Lee, F. C., "Isolated Three-Phase Soft-Switching Rectifier/Regulator," Virginia Power Electronics Center Project Rept. I-270, Virginia Polytechnic Inst. and State Univ., Blacksburg, VA, June 1999.

[6]Kassakian, J. G., Schlecht, M. F., and Verghese, G. C., *Principles of Power Electronics*, Addison Wesley Longman, Reading, MA, 1991, pp. 103–109.

[7]Middlebrook, R. D., "Input Filter Considerations in Design and Application of Switching Regulators," IEEE Industry Application Society Annual Meeting, Oct. 1976, Chicago, IL, Republished in "Advances in Switch-Mode Power Conversion, Vol. I and II," 2nd edition TESLAco, 1987, Paper 7, pp. 91–107.

[8]Vanderplaats, G. N., *Numerical Optimization Techniques for Engineering Design*, Vanderplaats R and D, Inc., Colorado Springs, CO, 1988, pp. 229–241.

[9]Haftka, R. T., and Gürdal, Z., *Elements of Structural Optimization, Third Revised and Expanded Edition*, Kluwer Academic Publishers, Dordrecht, The Netherlands, 1992, pp. 182–186.

[10]Ogata, K., *Modern Control Engineering*, Eastern Economy ed. Prentice–Hall, Upper Saddle River, NJ, 1986, pp. 527, 528.